Composite solitons in ^{3}He-A in the presence of superflow

Dieter Vollhardt* and Kazumi Maki
Department of Physics, University of Southern California, Los Angeles, California 90007
(Received 8 March 1979)

We have studied theoretically the effect of superflow on the composite solitons in ^{3}He-A for $\vec{H} \parallel \vec{v}_s$ and $\vec{H} \perp \vec{v}_s$. Here $\vec{H}$ is a static magnetic field and $\vec{v}_s$ is the superfluid velocity. The domain-wall energy as well as related NMR satellite frequencies are determined as functions of v_s. In the parallel geometry ($\vec{H} \parallel \vec{v}_s$), we predict hysteresis in the satellite frequencies when the superfluid velocity v_s is changed, due to the existence of two branches of stable textures. In both configurations there exist critical velocities $v_s (\lesssim 1$ mm/sec), at which the domain-wall energy becomes negative indicating the global instability of the uniform texture.

I. INTRODUCTION

Textures in superfluid ^{3}He-A are of current interest. The simplest among them are domain-wall-like textures[1,2] (composite solitons), which are stable in a strong magnetic field[3] ($H >> H_0 \simeq 20$ Oe). The existence of composite solitons has been verified by the appearance of satellite frequencies in NMR experiments.[4,5]

The domain-wall configuration may be modified by a variety of external perturbations. The object of the present paper is to study the effect of superflow on the composite solitons in ^{3}He-A, which can be readily tested experimentally.

Textures in ^{3}He-A are characterized by two unit vectors $\hat{l}$ (which describes the symmetry axis of the quasiparticle energy gap) and $\hat{d}$ (the spin axis of the condensate). The superflow couples to the texture via the anisotropy energy and the torque energy; the former tends to align the $\hat{l}$ vector parallel to $\vec{v}_s$, the superfluid velocity field, while the latter introduces nonplanarity into the texture; the superflow tends to wind the $\hat{l}$ vector around the direction of the flow. The latter effect ultimately leads to the instability of the uniform texture.[6]

In the present paper we confine our analysis to two arrangements of $\vec{v}_s$ and $\vec{H}$; (i) the parallel case ($\vec{H} \parallel \vec{v}_s$) and (ii) the perpendicular case ($\vec{H} \perp \vec{v}_s$), where $\vec{H}$ is the static magnetic field. This magnetic field confines both the $\hat{l}$ and $\hat{d}$ vectors in the plane perpendicular to $\vec{H}$, in the absence of superflow.[1,2] The superflow then breaks the planarity of the $\hat{l}$ vector even in the high-field limit. For simplicity we limit our considerations to the case $\hat{k} \parallel \vec{v}_s$, where $\hat{k}$ is a unit vector normal to the domain wall, since in most of the experimental setups the smallest cross sectional area (favored by the domain wall) is likely to be perpendicular to the flow.

Within the present limit, we need four variables to characterize textures in ^{3}He-A; $\hat{l}$ and $\hat{d}$ and Φ, the phase of the order parameter where $\hat{d}$ is still confined in the plane perpendicular to $\vec{H}$. This leads to four coupled differential equations to determine the equilibrium texture, which have to be solved simultaneously—usually an unmanageable task. In this situation a variational approach is much more tractable.

Therefore, most of the calculations are done variationally except for a few situations, where the exact solutions are available. In these cases our variational solutions are compared with the exact ones, which shows that the errors are always within only a few percent. In the case of $\vec{v}_s \perp \vec{H}$, we find that the domain-wall energy first increases slightly as the superflow velocity v_s increases but then decreases monotonically, while for $\vec{v}_s \parallel \vec{H}$ the domain-wall energy always decreases monotonically until in both cases it eventually passes zero when $v_s \simeq \hbar/\sqrt{2} m \xi_\perp$ ($\simeq 1$ mm/sec), where m is the mass of ^{3}He atom and $\xi_\perp$ [$\equiv (2\rho_{S\perp}/\chi_N)^{1/2}/\Omega_A \simeq 14$ μm] is the dipolar coherence length. According to Landau's criterion, at this point, where the domain-wall energy vanishes, the uniform texture (in a strong magnetic field) becomes unstable against the formation of domain walls. In the parallel case ($\vec{H} \parallel \vec{v}_s$) the corresponding critical velocity is 0.88 of the critical velocity associated with the local instability of the uniform texture in this particular geometry ($\vec{H} \parallel \vec{v}_s$).[7] However, whether the present instability triggers the transformation of the uniform texture into another texture (say, the composite soliton lattice) or not can only be answered when the creation mechanism of the domain wall is clarified. We have also calculated the NMR satellite frequencies associated with the composite solitons as a function of the superflow velocity v_s. In both parallel and perpendicular cases, the transverse shift initially decreases monotonically as v_s increases. Then in the parallel case at $q = q_{c1}$ the shift jumps to a small value signaling a dramatic textural transformation to a bendlike pure $\hat{l}$ texture.[8] When the super-

flow is reduced at this point, however, the satellite frequency stays at the lower branch and varies only slightly; the satellite frequency should thus reveal a remarkable hysteresis behavior as a function of v_s. This is due to the local stability of the $\hat{l}$ texture for all v_s. The longitudinal satellite frequencies, on the other hand, increase initially with v_s in both configurations. Therefore, composite solitons provide an excellent superflow monitor *in situ*.

We believe that most of the satellite frequencies seen in ^{3}He-A in the presence of superflow by Flint *et al.*[9] are associated with the composite solitons considered here. For example, although none of their configurations correspond to the present cases under consideration, the observed transverse shift did decrease as v_s was increased as we have seen in our limited cases. We hope that we shall extend the present calculations to more general configurations with an arbitrary angle between $\vec{v}_s$ and $\vec{H}$ in the near future.

In Sec. II, we describe the free energy of the composite soliton (the domain-wall energy) in the presence of superflow. Section III is devoted to the calculation of the NMR resonance frequencies. The results are summarized in Sec. IV.

In all of the calculations reported here, the A-phase order parameter is given by $A_{\mu i}=\hat{d}_\mu\Delta_i$ with

$$\Delta_i=[\Delta_0/\sqrt{2}]e^{i\Phi}(\hat{\delta}_1+i\hat{\delta}_2)_i\ , \tag{1}$$

where $\hat{\delta}_1$, $\hat{\delta}_2$, and $\hat{l}(\equiv\hat{\delta}_1\times\hat{\delta}_2)$ constitute an orthonormal triad describing the orbital component and $\hat{d}$ represents a unit vector describing the spin component. The spatial variation of these vectors is determined in the Ginzburg-Landau regime[10] by the free energy $F=F_{\rm kin}+E_D$,

$$\begin{aligned}F_{\rm kin}=\tfrac{1}{2}K\int d^3r\,[3|\vec{\nabla}\cdot\vec{\Delta}|^2&\\+|\vec{\nabla}\times\vec{\Delta}|^2+2|\vec{\Delta}\cdot\vec{\nabla})\hat{d}|^2&\\+|\vec{\Delta}|^2(|\vec{\nabla}\cdot\hat{d}|^2+|\vec{\nabla}\times\hat{d}|^2)]\ ,&\end{aligned} \tag{2}$$

where in the weak-coupling theory[10] K is given by

$$K=\frac{6}{5}\left(\frac{N}{8m^*}\right)\frac{7\zeta(3)}{(2\pi T_c)^2}\ .$$

For the domain wall with the normal vector parallel to the superflow $\vec{v}_s$ ($\parallel\hat{z}$), $\hat{l}$, $\hat{d}$, and $\vec{\Delta}$ are parameterized as

$$\hat{l}=\sin\chi(\cos\gamma\hat{x}+\sin\gamma\hat{y})+\cos\chi\hat{z}\ ,$$

$$\hat{d}=\sin\psi(\cos\phi\hat{x}+\sin\phi\hat{y})+\cos\psi\hat{z}\ ,$$

and

$$\begin{aligned}\vec{\Delta}=[\Delta_0/\sqrt{2}]e^{i\Phi}&\\\times\{-\sin\gamma\hat{x}+\cos\gamma\hat{y}&\\+i[\sin\chi\hat{z}-\cos\chi(\cos\gamma\hat{x}+\sin\gamma\hat{y})]\}\ ,&\end{aligned} \tag{3}$$

where Φ, χ, γ, ψ, and ϕ depend only on z.

Substituting Eq. (3) into Eq. (2), we obtain

$$\begin{aligned}\mathfrak{F}=\tfrac{1}{2}A\{&2(1+\sin^2\chi)\Phi_z^2+(1+\cos^2\chi)\gamma_z^2\\&-4\cos\chi\Phi_z\gamma_z+(1+2\cos^2\chi)\chi_z^2\\&+2(1+\sin^2\chi)(\psi_z^2+\sin^2\psi\phi_z^2)\\&+4\xi_1^{-2}[\sin^2\upsilon+4\Omega(\cos\upsilon-\Omega)]\}\ ,\end{aligned} \tag{4}$$

where $\upsilon=\chi-\psi$,

$$\Omega=\sin\chi\sin\psi\sin^2[\tfrac{1}{2}(\gamma-\phi)]\ ,$$

and the suffix z on Φ, χ, etc., implies the derivative with respect to z.

Here $\mathfrak{F}$ is the free-energy density and $A=\frac{1}{2}K\Delta_0^2$. Since Φ is a cyclic variable we have

$$\frac{d}{dz}[(1+\sin^2\chi)\Phi_z-\cos\chi\gamma_z]=0\ . \tag{5}$$

In particular, in the presence of a uniform flow in the z direction with momentum q, Eq. (5) is solved as

$$\Phi_z=(q+\cos\chi\gamma_z)(1+\sin^2\chi)^{-1}\ . \tag{6}$$

In the presence of uniform flow, it is more appropriate to consider the Gibbs potential $\mathcal{G}=\mathfrak{F}-\Phi_z(\partial\mathfrak{F}/\partial\Phi_z)$, where Φ_z is eliminated by Eq. (6). This yields

$$\begin{aligned}\mathcal{G}=\tfrac{1}{2}A\Bigg[&-\frac{2q^2}{1+\sin^2\chi}+\frac{\sin^2\chi(3-\sin^2\chi)}{1+\sin^2\chi}\gamma_z^2\\&-\frac{4\cos\chi q\gamma_z}{1+\sin^2\chi}+(1+2\cos^2\chi)\chi_z^2\\&+2(1+\sin^2\chi)(\psi_z^2+\sin^2\psi\phi_z^2)\\&+4\xi_1^{-2}[\sin^2\upsilon+4\Omega(\cos\upsilon-\Omega)]\Bigg]\ .\end{aligned} \tag{7}$$

Finally, let us recall, that in the presence of a strong magnetic field $\vec{H}$ the $\hat{d}$ vector is constrained to the plane perpendicular to $\vec{H}$. Therefore, we have $\psi=\frac{1}{2}\pi$ for $\vec{H}\parallel\vec{v}_s$ and $\phi=0$ for $\vec{H}\perp\vec{v}_s$.

II. DOMAIN-WALL ENERGY

In the following we shall consider the two limiting cases separately:

A. Parallel geometry ($\vec{H}\parallel\vec{v}_s$)

In the absence of superflow, the exact composite soliton in this case is known.[1] This solution requires essentially only two parameters; a length η^{-1}, which

is the characteristic length scale (i.e., the domain wall thickness) over which the $\hat{l}$ vector deviates from the asymptotic value, which is of the order of $\xi_\perp$; and a parameter τ, which determines the angle by which $\hat{l}$ is twisted around. In the presence of superflow we shall consider a variational solution, which allows more degrees of freedom;

$$\cos\chi = -\lambda\,\mathrm{sech}(\rho\eta z), \quad \sin(\gamma/\tau) = \mathrm{sech}\eta z\ , \qquad \sin(\gamma-\phi) = \mathrm{sech}\eta z, \quad \psi = \tfrac{1}{2}\pi\ . \tag{8}$$

This variational solution contains the one for $q=0$; in this limit we have $\lambda=0$, $\rho=1$, $\tau=0.8$, and $\eta=\sqrt{5}\xi_\perp^{-1}$. In Eq. (8), λ and ρ are new parameters; λ allows $\hat{l}$ to have a component parallel to the flow while ρ dictates the new length scale associated with the nonplanarity of the $\hat{l}$ vector.

Substituting Eq. (8) into Eq. (7), the domain-wall energy per unit surface is obtained by

$$E_{\text{domain wall}} = 8A\,\xi_\perp^{-1}\,\tilde{g} = \tfrac{1}{2}\int_{-\infty}^{\infty} dz\,(\mathcal{G}-\mathcal{G}_0)\ , \tag{9}$$

where $\tilde{g}$ is the domain-wall energy normalized by the one for the $\hat{d}$ soliton, and $\mathcal{G}_0$ is the Gibbs potential for the uniform texture. For fixed q values Eq. (9) is minimized with respect to the variational parameters λ, ρ, η, and τ. The result is shown in Fig. 1 as a function of the superflow q. (Note that the superfluid velocity v_s is given in terms of q as $v_s=\hbar q/2m$; therefore, $q=\xi_\perp^{-1}$ corresponds to $v_s=\hbar\xi_\perp^{-1}/2m\simeq 0.71$ mm/sec.) For $q=0$ we recover the result $\tilde{g}=0.447$. As the superflow q increases, the free energy decreases slowly, while λ increases almost linearly with q so that the pure twist texture now acquires a bend around the middle of the domain wall (see Fig. 2). Simultaneously τ increases and ρ decreases slowly. At $q=q_{c1}(\equiv 0.638\xi_\perp^{-1})$ and $\tilde{g}=0.409$ the present solution becomes locally unstable, the instability being announced already for $q\lesssim q_{c1}$ by a sharp increase in λ. At this point λ and τ jump to unity, while ρ goes to zero and η diverges so that $\rho\eta$ is finite; the texture makes a transition to a different configuration, which is stable and has a much smaller domain-wall energy. The new texture is planar and is a pure $\hat{l}$ texture[8] (i.e., $\hat{d}$ stays constant throughout the domain wall). The reason why this configuration is energetically so favorable can easily be understood. $\tau=1$ and $\eta\to\infty$ implies that the twisting of half of the texture takes place only in a very narrow region so it can take full advantage of the torque energy. However, this does not lead to a very high gradient energy as the turning occurs when $\hat{l}$ is almost parallel to the flow ($\lambda=1$). These textures are sketched in Fig. 3. The twist composite soliton for $q=0$ is shown in (a); in the presence of superflow $\hat{l}$ acquires a small bend (i.e., a finite component into the flow direction) (b); it finally transforms into the pure $\hat{l}$ texture for $q\geq q_{c1}$, (c). When q is further increased the free energy of this soliton decreases almost linearly with q mainly due to the torque energy and ultimately the domain-wall energy becomes negative for $q>q_{c2}(\equiv 0.893\xi_\perp^{-1})$. It is important to point out that if the superflow is decreased after the transition into the $\hat{l}$ texture, the domain wall stays on the $\hat{l}$ texture in the whole range of $q(0<q<q_{c2})$, although for small q the domain-wall energy of the $\hat{l}$ texture becomes higher than that of the composite soliton we have started with (see Fig. 1). This is because the pure $\hat{l}$ texture is a local minimum of the free energy and to bring down the $\hat{l}$ texture to the composite soli-

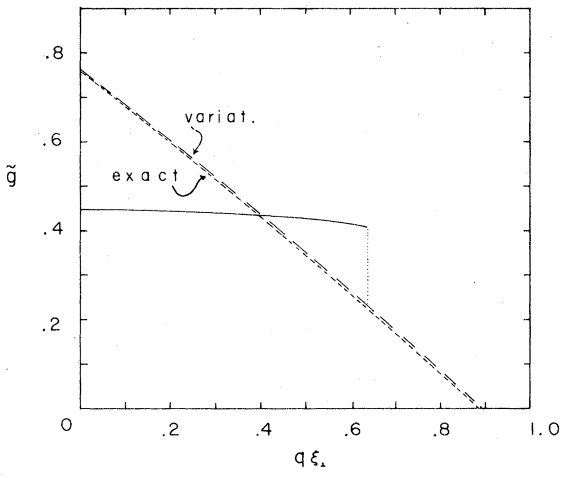

FIG. 1. Domain-wall energies for $\vec{H}\|\vec{v}_s$ are shown as functions of the superflow, $q\xi_\perp$ [$\equiv v_s/v_0$, with $v_0\equiv(\hbar/\sqrt{2}m)\xi_\perp^{-1}\simeq 1$ mm/sec]. The solid curve is due to the solution that connects smoothly to the twist soliton for $q=0$, while the broken curve represents the planar $\hat{l}$ textures.

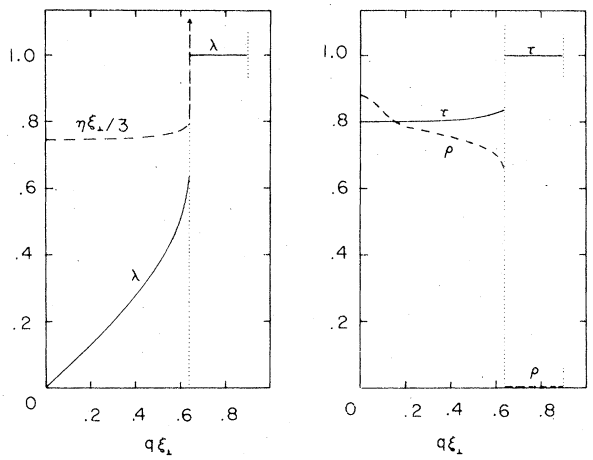

FIG. 2. Parameters describing the composite soliton for $\vec{H}\|\vec{v}_s$ are shown as functions of $q\xi_\perp$.

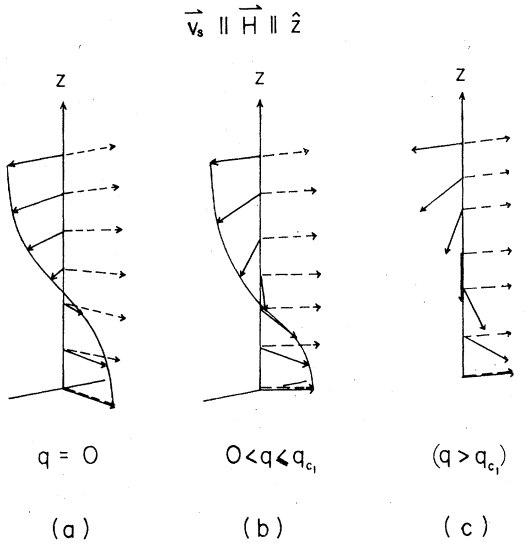

FIG. 3. Spatial conformations of three typical domain walls are shown schematically. (a) The twist soliton for $q=0$, (b) the twist soliton with a mixture of bend in $\hat{l}$, and (c) the planar $\hat{l}$ texture. Here the solid arows indicate the direction of $\hat{l}$, while the broken arrows indicate that of $\hat{d}$.

ton it appears to require a large perturbation to the system; we expect therefore a remarkable hysteresis when q is first increased and then decreased, which should be readily monitored by the NMR satellites (see Sec. III).

In the case of the pure $\hat{l}$ texture, the domain-wall energy as well as the solution are obtained analytically, which are given in Appendix A. However, for our purpose of determining the satellite frequencies, variational solutions are more convenient. Furthermore, we can test the accuracy of the variational solution against the exact solution in the present case. As to the variational solution we take again Eq. (8) with $\lambda=1$, $\tau=1$, $\rho\to 0$, $\eta\to\infty$, and $\eta\rho=\zeta$. With this ansatz the normalized domain wall energy is easily obtained from Eq. (8)

$$\tilde{g}=\tfrac{1}{2}\{\tfrac{7}{3}[1-\tfrac{1}{16}\pi(q\xi_\perp)^2]\}^{1/2}-\tfrac{1}{4}\pi q\xi_\perp\ , \qquad (10)$$

with

$$\zeta^{-1}=2\{\tfrac{3}{7}[1-\tfrac{1}{16}\pi(q\xi_\perp)^2]\}^{-1/2}\xi_\perp\ .$$

The above domain-wall energy is compared with the exact value in Appendix A. As expected, the variational value is slightly higher than the exact value. However, as seen in Fig. 1, the energy difference is always less than 2% of the wall energy at $q=0$, which is quite reassuring. As already mentioned Eq. (10) tells that $\tilde{g}$ vanishes for $q=q_{c2}$, while at this point ζ is still finite. This feature is in strong contrast to the case of the perpendicular geometry where the soliton delocalizes at the critical value of q.

B. Perpendicular geometry ($\vec{H}\perp\vec{v}_s$)

In this case we assume that the magnetic field points in the y direction. Again we choose a variational ansatz, which is a generalization of the one for $q=0$ to accommodate the additional effects of a superflow on the texture

$$\sin\upsilon=\operatorname{sech}\eta z\ ,$$
$$\chi=\alpha\upsilon+(1-\alpha)\sin^{-1}[\operatorname{sech}(\rho\eta z)]\ , \qquad (11)$$
$$\gamma=2(a-b\sin\chi),\quad \phi=0\ ,$$

where $\upsilon=\chi-\psi$.

Here η, α, ρ, a, and b are variational parameters, which have the following physical meaning: (i) η^{-1} is again the length over which the angle between $\hat{l}$ and $\hat{d}$ varies from 0 to π (mostly governed by the nuclear dipolar energy). (ii) At $q=0$, α describes the asymptotic orientation of $\hat{l}$ outside the domain wall. In the presence of superflow α no longer gives the asympotic configuration; however it still describes the reminant tendency. (iii) ρ^{-1} stands for the second length scale introduced by the superflow, (iv) $2a$ is the azimuthal angle of $\hat{l}$ in the asymptotic region and finally, (v) $2b$ depicts the winding angle of $\hat{l}$ to take advantage of the torque energy due to the superflow. It should be made clear from the outset that the composite soliton in the present geometry ($\vec{H}\perp\vec{v}_s$) is globally unstable in the presence of superflow; there exists a solution with $\hat{l}$ continuously delocalized but with large winding, which has a domain-wall energy unbounded from below (the domain-wall energy becomes $-\infty$ as the size of the domain wall becomes infinite). The proof is given in Appendix B. However, for small q, the solution which leads to this instability (which we shall label from now on as the delocalized solution) lies quite far away in the functional space from the solution that can be obtained by a small modification of the equilibrium solution at $q=0$. Therefore, we believe that in an actual experiment the latter texture is more relevant and we shall concentrate on it from now on.

Substituting Eq. (11) into Eq. (9), we have minimized $\tilde{g}$ with respect to the parameters η, α, ρ, a, and b. For small q we can expand Eq. (9) in powers of $q\xi_\perp$. In this limit $\rho=0.307q\xi_\perp$, while a and b increase quadratically with $(q\xi_\perp)$. This implies that a small superflow has mainly two effects: (i) it aligns $\hat{l}$ parallel to $\vec{v}_s$ at a distance of the order of q^{-1} from the center of the domain wall, (ii) it slightly tilts $\hat{l}$ out of the plane perpendicular to the magnetic field. (This is schematically shown in Fig. 4.) The normalized domain-wall energy $\tilde{g}$ and the variational parameters are shown as functions of q in Figs. 5 and 6, respectively. The energy initially increases slightly with increasing q but then drops monotonically as q is further increased. At $q=q_c(\equiv 0.77\xi_\perp^{-1})$ the solution

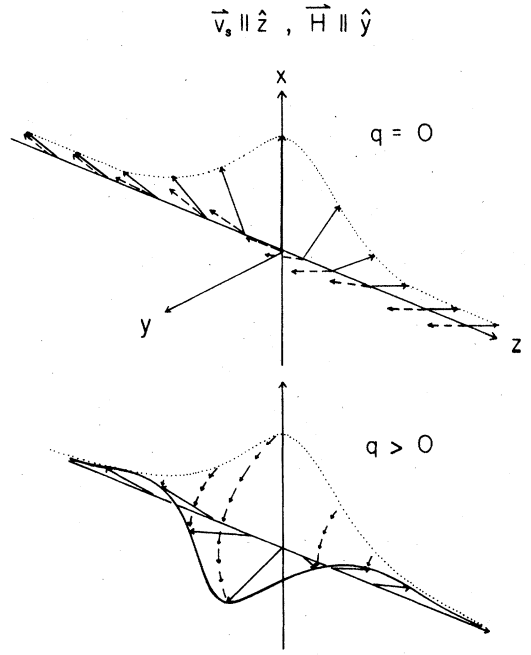

FIG. 4. Spatial conformations of the splay soliton for $q=0$ and $q \neq 0$ are shown schematically. Here solid arrows indicate the direction of $\hat{l}$. As the superfluid velocity increases the central part of $\hat{l}$ begins to wind around $\vec{v}_s$, as indicated by small arrows.

becomes locally unstable against unlimiting winding of $\hat{l}$ around $\vec{v}_s$ and the texture delocalized. In other words at this point ($q=q_c$), the potential barrier in the functional space, which separates the equilibrium soliton and the delocalized solution, suddenly disappears. The solution we have just analyzed is characterized by an antisymmetric configuration of the $\hat{d}$ vector, $\psi(-z)=-\psi(z)$, which is the unique way to

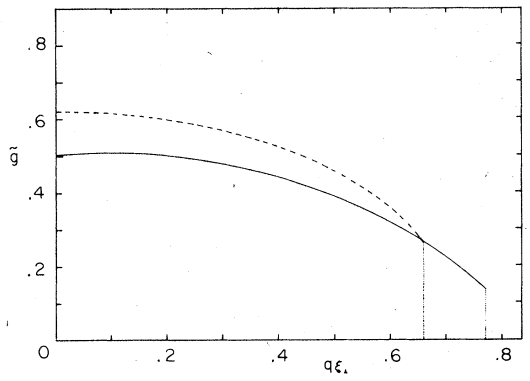

FIG. 5. Domain-wall energies for $\vec{H} \perp \vec{v}_s$ as functions of $q\xi_\perp$. The solid curve corresponds to the domain wall with asymmetric $\hat{d}$ configuration, the broken curve for the one with symmetric $\hat{d}$. The latter domain-wall energy is always larger than the former.

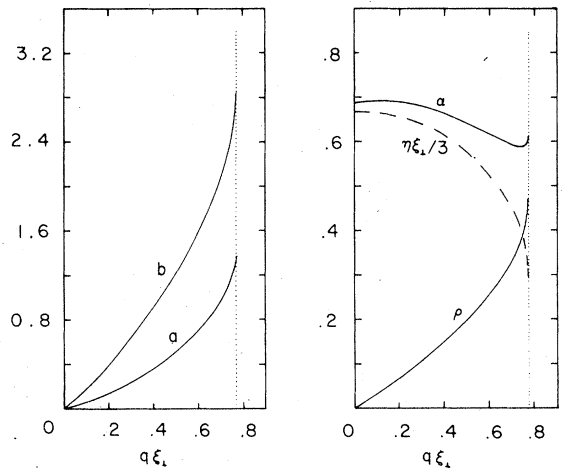

FIG. 6. Parameters describing the splay composite soliton ($\vec{H} \perp \vec{v}_s$) are shown as functions of $q\xi_\perp$.

have a symmetric dipole energy. We have, however, also examined other configurations in which $\hat{d}$ is symmetric, $\psi(-z)=\psi(z)$, for instance

$$\sin(\chi-\psi)=\operatorname{sech}\eta z \ ,$$
$$\sin\psi=\lambda\operatorname{sech}(\rho\eta z) \ ,$$
$$\gamma=2(a-b\sin\chi) \ , \tag{12}$$

where ρ, η, λ, a, and b are again variational parameters.

This solution has always higher domain-wall energy and a smaller critical velocity, where the domain wall becomes locally unstable. The domain-wall energy of this variational solution is also shown in Fig. 5. In contrast to the case of the parallel geometry, all of these solutions become locally unstable at finite q's.

III. MAGNETIC RESONANCE

Nuclear magnetic resonance experiments[4,5] have been crucial for the identification of the composite solitons in ^{3}He-A. In general the domain wall in ^{3}He-A carries a local deficit of nuclear dipole energy. As already shown elsewhere,[1,2] a domain wall gives rise to potential wells for the spin oscillations; they accommodate just one bound state for both the longitudinal and transverse mode. The bound spin-wave spectrum then provides a unique probe of the spatial configuration of the domain wall involved.

A. Parallel geometry ($\vec{H} \parallel \vec{v}_s$)

In this case we shall first write $\hat{d}$ as

$$\hat{d}=\cos g[\cos(\phi+f)\hat{x}+\sin(\phi+f)\hat{y}]-\sin g\hat{z} \ , \tag{13}$$

where ϕ is given by the equilibrium $\hat{d}$ configuation, Eq. (8) and f and g describe the fluctuation around the equilibrium $\hat{d}$.

Replacing ϕ and ψ in Eq. (7) by $\phi+f$ and $\psi+g$, we expand it in powers of f and g. Retaining the quadratic terms in f and g only, we can construct the fluctuation free energy. Then the eigenvalues associated with the f and g oscillation are related to the satellite resonance frequencies by[1]

$$\omega_l^s=\lambda_f^{1/2}\Omega_A,\quad \omega_t^s=(\omega_0^2+\lambda_g\Omega_A^2)^{1/2},$$

where ω_l^s, and ω_t^s are the longitudinal and transverse satellite frequencies, Ω_A is the longitudinal resonance frequency of bulk ^{3}He-A, and ω_0 is the Larmor frequency. The eigenvalues λ_f and λ_g are given by

$$\lambda_f f=-\tfrac{1}{2}\xi_\perp^2\frac{\partial}{\partial z}[(1+\sin^2\chi)f_z]+\sin^2\chi[1-2\sin^2(\gamma-\phi)]f\ , \tag{14}$$

$$\lambda_g g=-\tfrac{1}{2}\xi_\perp^2\frac{\partial}{\partial z}[(1+\sin^2\chi)g_z]+[\sin^2\chi\cos^2(\gamma-\phi)-\cos^2\chi-\tfrac{1}{2}\xi_\perp^2(1+\sin^2\chi)\phi_z^2]g\ . \tag{15}$$

Substituting χ, γ, and ϕ given in Eq. (8), we have solved Eqs. (14) and (15) variationally, by assuming that $f\propto\mathrm{sech}^\nu(\eta z)$ and $g\propto\mathrm{sech}^\mu(\eta z)$ where ν and μ are variational parameters. The eigenvalues are determined as functions of q and shown in Fig. 7. In the figure we denote λ_f and λ_g by λ_l and λ_t, respectively, as the former appears in the longitudinal resonance, the latter in the transverse resonance. λ_l increases slowly as q increases and then suddenly jumps up at $q=0.636\xi_\perp^{-1}$, at the textural transformation into a pure $\hat{l}$ texture. Similarly λ_t initially decreases slowly and then jumps down to a smaller value at $q=q_{c1}$. The corresponding values of λ_l and λ_t for the pure $\hat{l}$ texture are also determined variationally and shown in Fig. 7. These λ_l and λ_t continue smoothly beyond $q=q_{c2}$, where $\hat{g}$ becomes 0. Therefore, this point does not correspond to any instability of the domain wall. When q is decreased from $q>q_{c1}$, the texture always appears to be an $\hat{l}$ texture and λ_l and λ_t go back smoothly to those corresponding to the pure $\hat{l}$ texture with $q=0$ (hysteresis behavior). Therefore the satellite frequencies in $0<q<q_{c1}$ can be completely different depending on how the domain walls are prepared. Furthermore, λ_l and λ_t at $q=0$ reproduce the earlier result,[8] although in the present situation λ_l and λ_t have to be interchanged. In the earlier calculations the magnetic field direction was taken to be in the y direction, while in the present calculation $\vec{H}$ is in the z direction. The stability of the present configuration is guaranteed by the superflow (in particular by the torque energy), which was absent in the earlier analysis.

We have tried to improve our λ_l and λ_t values by making use of variational functions with more than two variational parameters. However, all these functions failed to improve the present results by more than a fraction of one percent. Therefore we believe that the present result should be quite accurate; the errors should be within a few percent. We have also checked the accuracy of the potential energies obtained by the variational equilibrium solutions by comparing them to those given by the exact solutions in the case of pure $\hat{l}$ textures. In Fig. 8 both solu-

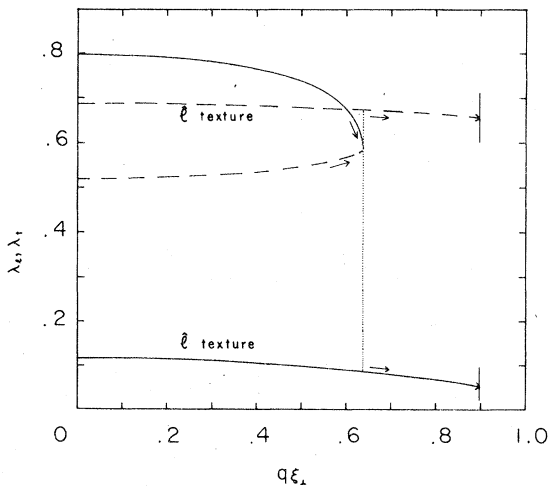

FIG. 7. Parameters λ_l (broken curves) and λ_t (solid curves), which describe the longitudinal and transverse satellite frequencies, are shown as functions of the superfluid velocity $q\xi_\perp=v_s/v_0$ for $\vec{H}\parallel\vec{v}_s$.

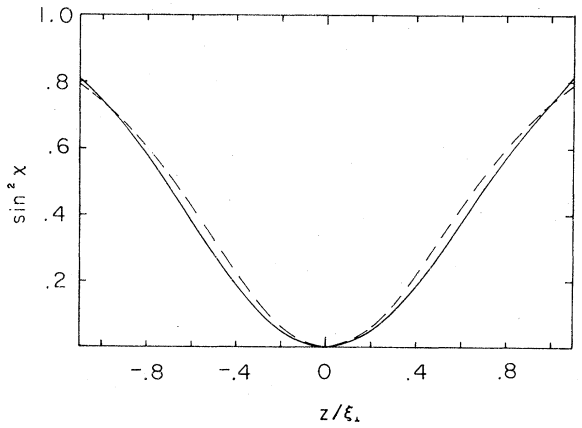

FIG. 8. Potential for longitudinal $\hat{d}$ fluctuations given by the variational solution (broken curve) is compared with the one of the exact solution (solid curve) for $q\xi_\perp=0.4$ and $\vec{H}\parallel\vec{v}_s$.

tions are shown for $q=0.4\xi_\perp^{-1}$. The agreement is similar for all other values of q $(0<q<q_{c2})$.

The predicted q dependences of λ_l and λ_t are rather weak in particular for small superflow, though the domain wall in ^{3}He-A would provide an excellent monitor of the superfluid velocity.

B. Perpendicular geometry ($\vec{H}\perp\vec{v}_s$)

In this case we write $\hat{d}$

$$\hat{d}=[\sin(\psi+f)\hat{x}+\cos(\psi+f)\hat{z}]\cos g+\sin g\hat{y}\ , \tag{16}$$

The eigenequations for f and g are given by

$$\lambda_f f=-\tfrac{1}{2}\xi_\perp^2\frac{\partial}{\partial z}[(1+\sin^2\chi)f_z]$$
$$+\{\cos 2\upsilon+4\sin\chi\sin^2\frac{\gamma}{2}$$
$$\times[\sin(\upsilon-\psi)-\sin\chi\sin^2\frac{\gamma}{2}\cos 2\psi]\}f\ , \tag{17}$$

$$\lambda_g g=-\tfrac{1}{2}\xi_\perp^2\frac{\partial}{\partial z}[(1+\sin^2\chi)g_z]$$
$$+[(\cos\upsilon-2\sin\chi\sin\psi\sin^2\frac{\gamma}{2})^2-\sin^2\chi\sin^2\gamma$$
$$-\tfrac{1}{2}\xi_\perp^2(1+\sin^2\chi)\psi_z^2]g\ . \tag{18}$$

Again the longitudinal and transverse satellite frequencies are expressed in terms of λ_f and λ_g, respectively. The eigenvalues are determined variationally with $f\propto\mathrm{sech}^\nu\eta z$ and $g\propto\mathrm{sech}^\mu\eta z$. (Variational functions with more than two parameters again could not improve upon this ansatz by more than a fraction of a percent.) The results are shown in Fig. 9. Here

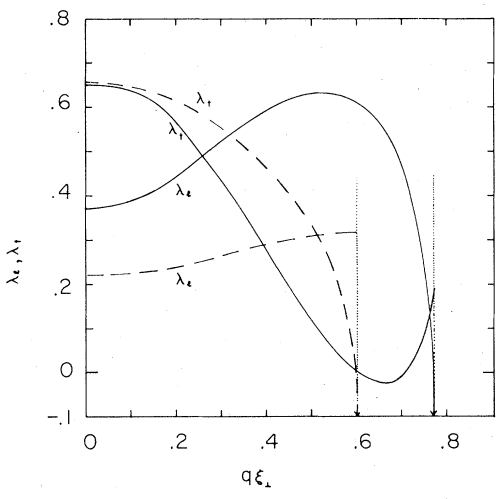

FIG. 9. λ_l and λ_t for $\vec{H}\perp\vec{v}_s$ are shown as functions of $q\xi_\perp$. Here solid curves correspond to the asymmetric $\hat{d}$ solution, the broken curves to the symmetric $\hat{d}$ solution.

again we denote λ_f and λ_g by λ_l and λ_t, respectively. The general q dependences of λ_l and λ_t are quite similar to the parallel case, although λ_l and λ_t depend more strongly on q in the present case. Furthermore, in the region near $q\simeq 0.6\xi_\perp^{-1}$, λ_t exhibits more structure. Ultimately at $q=q_c(\equiv 0.77\xi_\perp^{-1})$, λ_l jumps to $-\infty$ signaling the intrinsic instability of the domain wall. It appears that for $q>q_c$, there are no longer any stable domain-wall-like textures in sharp contrast to the case of the parallel geometry. In Fig. 9 we have also included λ_l and λ_t associated with the second texture [Eq. (12)] by broken curves. The general tendency of λ_t resembles that observed by the Florida group[9] for an intermediate geometry [e.g., angle $(\vec{H},\vec{v}_s)=45°$]. It appears that the domain wall is the only viable candidate for the satellite structure in the magnetic resonance in ^{3}He-A. All other textures seem to have too small intensities, if they are linear or pointlike. Furthermore, these other textures do not appear to exhibit any interesting NMR structure.[11]

IV. CONCLUDING REMARKS

Making use of a variational approach, the composite solitons in ^{3}He-A in the presence of superflow have been studied in two limiting geometries ($\vec{v}_s\parallel\vec{H}$ and $\vec{v}_s\perp\vec{H}$).

We find that (i) in the parallel geometry the domain-wall energy decreases monotonically with q until $q=q_{c1}(\equiv 0.638\xi_\perp^{-1})$, where the composite soliton transforms into a pure $\hat{l}$ texture. Once the $\hat{l}$ texture appears, the texture remains a pure $\hat{l}$ texture even if q is reduced, leading to hysteresis in the NMR signal. As q is increased beyond q_{c1}, the domain-wall energy decreases continuously and passes through zero at $q=q_{c2}(\equiv 0.893\xi_\perp^{-1})$. At this point the uniform texture becomes globally unstable against the creation of domain walls. However, whether this instability actually implies the local instability of the uniform texture or not is yet to be examined. (ii) In the perpendicular geometry we note that the domain wall itself becomes globally unstable in the presence of superflow. However, the (delocalized) solution leading to this instability is very far away in the functional space from the solution that is obtained by continuous modification of the equilibrium solution for $q=0$. Therefore, the composite soliton appears essentially stable at least for small q. As q is increased, the solution becomes suddenly locally unstable against unlimited winding of $\hat{l}$ at $q=q_c(\equiv 0.77\xi_\perp^{-1})$. (iii) We have also calculated the satellite resonance frequencies associated with these two textures. We believe that the composite solitons provide an excellent superflow monitor of ^{3}He-A *in situ*.

In the case of the parallel geometry, the stable tex-

ture beyond $q = q_{c2}$ can be a regular lattice of $\hat{l}$ textures, which individually have negative domain-wall energy but have positive mutual repulsion. This possibility is currently being examined.

ACKNOWLEDGMENT

One of us (D.V.) gratefully acknowledges a dissertation scholarship by the Studienstiftung des Deutschen Volkes. We have benefitted from discussions with Y. R. Lin-Liu and Mario Liu. This work was supported by the NSF under Grant No. DMR76-21032.

APPENDIX A: ANALYTICAL RESULTS FOR THE PURE $\hat{l}$ TEXTURE ($\vec{H} \| \vec{v}_s$)

Substituting $\phi = 0$, $\psi = \frac{1}{2}\pi$, and $\sin\gamma = \mathrm{sech}\eta z$ with $\eta \to \infty$ into Eq. (9), we find the domain-wall energy in the presence of superflow;

$$\tilde{g} = \tfrac{1}{16}\xi_\perp \int_{-\infty}^{\infty} dz \left[(1+2\cos^2\chi)\chi_z^2 - q^2 \frac{\cos^2\chi}{1+\sin^2\chi} + 4\xi_\perp^{-2}\cos^2\chi \right] - \tfrac{1}{4}\pi q \xi_\perp , \tag{A1}$$

where the last term is obtained from

$$\lim_{\eta\to\infty} \int_{-\infty}^{\infty} \frac{q\cos\chi}{1+\sin^2\chi}\gamma_z = \frac{\pi\cos\chi(0)q}{1+\sin^2\chi(0)} \tag{A2}$$

(by this the torque energy is maximized). The Euler-Lagrange equation for χ is easily integrated. For an isolated domain wall, we have

$$\chi_z^2 = 4\xi_\perp^{-2}\cos^2\chi\left[1 - \frac{1}{4}\frac{(q\xi_\perp)^2}{1+\sin^2\chi}\right](1+2\cos^2\chi)^{-1} , \tag{A3}$$

which yields

$$2\xi_\perp^{-1}z = \int_0^\chi d\phi \frac{1}{\cos\phi} \times \left[\frac{(1+2\cos^2\phi)(2-\cos^2\phi)}{1+\sin^2\phi - \frac{1}{4}(q\xi_\perp)^2}\right]^{1/2} . \tag{A4}$$

In Fig. 8 the potential for the longitudinal mode $V_l(z) \propto 1-\sin^2\chi$ is shown as a function of z, for $q = 0.4\xi_\perp^{-1}$, which is compared with the variational one, $\sin^2\chi = \tanh^2\eta z$. Eliminating χ_z from Eq. (A1) we have

$$\tilde{g} = \tfrac{1}{2}\int_0^1 dy \left[(3-2y^2)\left[1 - \frac{(q\xi_\perp)^2}{4(1+y^2)}\right]\right]^{1/2} - \tfrac{1}{4}\pi q\xi_\perp . \tag{A5}$$

Finally, the first integral is integrated numerically and shown in Fig. 1. Equation (A5) is compared with the variational result Eq. (10) in the text.

APPENDIX B: GLOBAL INSTABILITY OF THE COMPOSITE SOLITON IN THE PRESENCE OF SUPERFLOW ($\vec{H} \perp \vec{v}_s$)

To see that there exists a class of localized solutions which leads to global instability, as an example we take a variational ansatz

$$\sin\chi = \mathrm{sech}\eta z, \quad \phi = 0, \quad \psi = \tfrac{1}{2}\pi ,$$

and

$$\gamma = -b^3\,\mathrm{sech}(\eta z/b) . \tag{B1}$$

Furthermore, we concentrate on the limit $b \to \infty$. The present ansatz describes a localized pure $\hat{l}$ texture, which is strongly wound up around the direction of superflow. Substituting Eq. (B1) into the domain-wall energy Eq. (9), we obtain

$$\tilde{g} = \tfrac{1}{8}(\eta\xi_\perp)[\mu + O(b^{-2})]b^2 + \tfrac{1}{2}(\eta\xi_\perp)^{-1}[1+c(q\xi_\perp)^2] - \tfrac{1}{2}(q\xi_\perp)b^3 , \tag{B2}$$

where

$$c = [\tfrac{1}{8}]^{1/2}\ln[\sqrt{2}+1] = 0.3116\ldots$$

and $\mu = 1.873$.

Eliminating η from Eq. (B2) we have

$$\tilde{g} = \tfrac{1}{2}b\{\mu[1+c(q\xi_\perp)^2]\}^{1/2} - \tfrac{1}{2}(q\xi_\perp)b^3 \tag{B3}$$

and

$$\eta = 4\xi_\perp^{-1}[1+c(q\xi_\perp)^2]/b^2 . \tag{B4}$$

From Eq. (B3) we see immediately that, for *any* $q > 0$, $\tilde{g}$ can be arbitrarily negative as b increases. Since b describes the winding of $\hat{l}$ as well as the spatial extension of the winding, $b \to \infty$ corresponds to a completely delocalized solution Eq. (B4). However, the above estimate is only valid for $b \gg 1$. On the other hand, the localized solutions we are interested in have rather small $b (\lesssim \pi)$. In these solutions b only starts to increase rapidly when q approaches q_c, where the domain wall becomes locally unstable.

*Address as of Sept. 1979: Max-Planck-Institut für Physik und Astrophysik, 8000 München 40, W. Germany.

[1]K. Maki and P. Kumar, Phys. Rev. Lett. 38, 577 (1977); Phys. Rev. B 16, 182 (1977).

[2]K. Maki and P. Kumar, Phys. Rev. B 17, 1088 (1978).

[3]V. P. Mineyev and G. E. Volvik, Phys. Rev. B 18, 3197 (1978).

[4]O. Avenel, M. E. Bernier, E. J. Varoquaux, and C. Vibet, in *Proceedings of the XIV International Conference on Low Temperature Physics, Otaniemi, Finland, 1975,* edited by M. Krusius and M. Vuorio (North-Holland, Amsterdam, 1975), Vol. 5, p. 429.

[5]C. M. Gould and D. M. Lee, Phys. Rev. Lett. 37, 1223 (1976).

[6]P. Bhattacharyya, T. L. Ho, and N. D. Mermin, Phys. Rev. Lett. 39, 1290 (1977); M. C. Cross and M. Liu, J. Phys. C 11, 1795 (1978).

[7]C. M. Cross (private communication); Y. R. Lin-Liu and K. Maki (unpublished).

[8]K. Maki and P. Kumar, Phys. Rev. B 16, 174 (1977).

[9]E. B. Flint, R. M. Mueller, and E. D. Adams, J. Low Temp. Phys. 33, 43 (1978).

[10]V. Ambegaokar, P. G. de Gennes, and D. Rainer, Phys. Rev. A 9, 2676 (1974).

[11]R. Bruinsma and K. Maki, Phys. Rev. B 18, 1101 (1978).